

The interaction of 3C 401 with the surrounding intracluster medium

Christopher S. Reynolds,^{1*} Laura W. Brenneman¹ and John T. Stocke²

¹*Department of Astronomy, University of Maryland, College Park, MD 20742, USA*

²*Department of Astrophysics and Planetary Science, University of Colorado, Boulder, CO 80309, USA*

Accepted 2004 November 21. Received 2004 November 10; in original form 2004 September 10

ABSTRACT

We present an observation of the radio galaxy 3C 401 and the surrounding intracluster medium (ICM) of its host galaxy cluster by the *Chandra X-ray Observatory*. This luminous radio galaxy is notable in that it has characteristics intermediate between the Fanaroff–Riley type I and II morphologies. We clearly detect point-like emission coincident with the radio core of 3C 401, although the spatial resolution of even *Chandra* is only 2 kpc at the distance of 3C 401 ($z = 0.201$) and so the possibility remains that this is a dense (and rapidly cooling) thermal gaseous core in the centre of the ICM atmosphere. Strong departures from spherical symmetry in the central 10–20 kpc of the ICM clearly suggest interaction between the ICM and the radio lobes of 3C 401. A central X-ray bar probably results from the evacuation of two ICM cavities by the expanding radio lobes. Beyond these central regions, the cluster possesses a flatter profile than many clusters of comparable mass, suggesting the importance of ICM heating and entropy injection by 3C 401. We detect an interesting cross-like structure in the ICM on 100 kpc scales. We speculate that this could be a radio-galaxy-induced disturbance corresponding to a time when 3C 401 was substantially more powerful. A particularly exciting possibility is that this cross-like structure corresponds to a large-scale global g-mode oscillation excited by a past outburst of 3C 401.

Key words: galaxies: clusters: general – quasars: individual: 3C 401 – X-rays: galaxies: clusters – X-rays: individual: 3C 401.

1 INTRODUCTION

The classic ‘cooling flow problem’ (Fabian 1994), the discrepancy between the observed radiative cooling rate of the intracluster medium (ICM) in rich galaxy clusters and the amount of cold gas or star formation actually observed, has obvious connections to galaxy formation. One can rephrase the cooling flow issue into the question: ‘Why are the cD galaxies in rich clusters not still in the process of forming?’ It seems clear that some agent must be heating the ICM core of rich clusters in order to (on average) balance the radiative cooling, and an obvious candidate for that agent is active galactic nucleus (AGN) activity. In other words, radio galaxy–ICM interactions may well be the agent that terminates the formation of the most massive galaxies (Benson et al. 2003; Binney 2004).

While a few examples of radio galaxy–ICM interactions were known in the *Einstein* and *ROSAT* days, it took the superior imaging capability of the *Chandra X-ray Observatory* to reveal the full complexity and ubiquity of this phenomenon. For example, Perseus A (Fabian et al. 2000, 2003), Hydra A (McNamara et al. 2000; David et al. 2001; Nulsen et al. 2002), Abell 2052 (Blanton et al. 2001) and Cygnus A (Smith et al. 2002) all show well-defined cavities in the X-ray-emitting gas that are coincident with the current radio

lobes of the central radio galaxy. In these sources, it is clear that the radio lobes have displaced the X-ray-emitting gas, producing the observed X-ray/radio anticoincidence. Bîrzan et al. (2004) have used an analysis of 16 clusters with cavities to find a significant correlation between the mechanical energy required to create the cavities and the radio power level of the central radio source. The existence of this correlation is strong evidence that the radio source is responsible for evacuating these cavities. Additionally, in at least 50 per cent of the cases studied, the mechanical energy estimated to be present in the cavities is sufficient to offset the estimated cooling of the cluster core. *Chandra* has also revealed the presence of ‘ghost’ cavities, i.e. X-ray cavities that are *not* coincident with the active radio lobes. In the Bîrzan et al. (2004) study the ‘ghost cavities’ have significantly larger estimated mechanical energies than cavities containing current-outburst radio source lobes. Examples include the outer cavity of Perseus A (Fabian et al. 2000, 2003), Abell 2597 (McNamara et al. 2001), NGC 4636 (Jones et al. 2002) and Abell 4059 (Heinz et al. 2002; Choi et al. 2004). In these sources, it is believed that the cavities are associated with old radio lobes (related to previous cycles of AGN activity). The low-frequency (74 MHz) synchrotron radio emission expected within this scenario has been observed from the ghost cavity of Perseus A (Fabian et al. 2002).

If one is interested in assessing the wider importance of radio galaxy–ICM interactions (e.g. to galaxy formation processes), it

*E-mail: chris@astro.umd.edu

is of obvious use to extend the study to powerful radio galaxies beyond our Local Universe. In this paper, we describe an observation of the moderately powerful ($P_{20\text{cm}} = 5 \times 10^{26} \text{ W Hz}^{-1}$) radio galaxy 3C 401 ($z = 0.201$) by *Chandra*. Despite having Fanaroff–Riley type II (FR II) radio power, this source has been classified as intermediate between an FRI and FR II morphologically (Harvanek & Stocke 2002), raising the possibility that it might be an example of a fading radio source. Specifically, 3C 401 contains no highly concentrated ‘hotspots’ at the leading edges of its two lobes, and the brightest portion of its extended structure is a luminous jet in the southern lobe. These characteristics are more similar to those of typical FRIs than FR IIs. 3C 401 is also much broader compared to its length than a typical FR II – thus, the nickname given to sources with this morphology: ‘fat doubles’. See Harvanek & Stocke (2002) for an identification and discussion of other ‘fat doubles’, including Hercules A. 3C 401 is surrounded by a cluster of galaxies with optical galaxy density (with the galaxy–galaxy two-point correlation function $B_{\text{gg}} \approx 1100 \text{ Mpc}^{1.77}$; Harvanek et al. 2001), equivalent to Abell richness class I–II. Harvanek et al. (2001) found that ‘fat doubles’ are found exclusively in clusters of galaxies at intermediate redshift.

The goal of the *Chandra* observation reported in this paper was to search for and characterize any interaction between this radio galaxy and the ICM of its host galaxy cluster. Clear signatures of this interaction were found. Section 2 describes the observation and our data reduction. Both our spectral and imaging results are presented in Section 3, and placed into a wider context in Section 4. Our conclusions are drawn in Section 5. Assuming the *WMAP* cosmology (flat universe with $\Omega_{\Lambda} = 0.73$, $H_0 = 71 \text{ km s}^{-1} \text{ Mpc}^{-1}$; Spergel et al. 2003) gives a luminosity distance of 976 Mpc, an angular size distance of 678 Mpc, and a look-back time of 2.42 Gyr.¹ At this distance, 1 arcsec subtends a linear distance of 3.38 kpc.

2 CHANDRA OBSERVATIONS AND DATA REDUCTION

The 3C 401 system was observed by *Chandra* on 2002 September 20 (22.7 ks exposure; obs-id 3083) and September 21 (24.9 ks exposure; obs-id 4370). The core of 3C 401 was centred 1 arcmin from the aim point on the S3 back-illuminated ACIS chip (7) such that the core of its cluster could be imaged entirely by the S3 chip. These observations were taken in imaging mode, i.e. the diffraction gratings are not placed in the X-ray path. The two level-2 events files for these two observations were merged using the MERGE_ALL script, and then filtered so as to include only events with ASCA grades 0, 2, 3, 4 and 6. Exposure-corrected images and spectra were created following the standard process outlined in the *Chandra* Interactive Analysis of Observations (CIAO) analysis threads.² All ACIS data reduction was performed using the CIAO version 3.0, and spectral analysis was performed using version 11.3 of the XSPEC fitting package.

3 RESULTS

3.1 Large-scale X-ray image

Fig. 1 shows an adaptively smoothed three-colour *Chandra* image of the general region surrounding 3C 401, overlaid with contours of

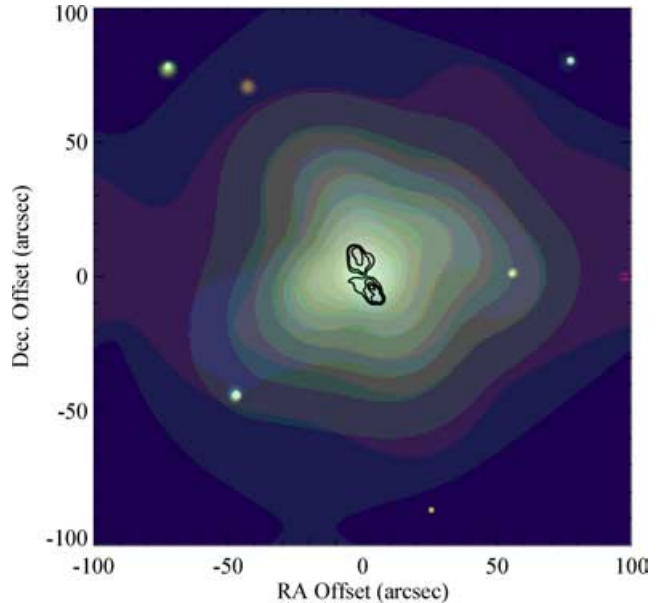


Figure 1. Adaptively smoothed three-colour *Chandra*/ACIS-S image of the 3C 401 cluster overlaid with contours of 20-cm radio emission from MERLIN. Note the cross-like structure displayed by the ICM. See text for a discussion of how this image was constructed and the robustness of the cross-like structure. North is up in this image. Please note that the colour image is only available in the electronic publication.

20-cm emission from MERLIN.³ To produce this X-ray image, we first extracted and exposure-corrected images from the cleaned filtered level-2 events file in three bands: 0.3–0.8 keV (soft), 0.8–2 keV (medium) and 2–10 keV (hard). The total image (i.e. the sum of the three bands) was adaptively smoothed using a $3\text{--}4\sigma$ smoothing kernel, and the resulting map of smoothing lengths was then applied to each of the images in the three bands separately. The three images are then overlaid to form the three-colour image, with red, green and blue denoting the soft, medium and hard band images, respectively. At the distance of 3C 401, this image covers a square region 680 kpc on a side. Please note that the colour image is only available in the electronic publication.

As can be seen from Fig. 1, we clearly detect an extended ICM halo centred on 3C 401, although we fail to detect any spatial variations in the hardness of the emission. Interestingly, the ICM appears to possess a cross-like structure, with four almost perpendicular spurs extending in the north-north-east/east-south-east/south-south-west/west-north-west (NNE/ESE/SSW/WNW) directions. The NNE–SSW axis is exactly that defined by the radio jets of 3C 401. Given that this is an adaptively smoothed image, one might be concerned that these spurs extend approximately in the direction of the point sources also seen in the field. However, precisely the same spur pattern is observed if one first removes the point sources prior to producing the adaptive smoothing map. One might also be concerned about the validity of the exposure map used to produce these images. However, the spurs are seen in both exposure-corrected and non-exposure-corrected images, and the amplitude of variations across the spurs (30–50 per cent) is substantially greater than can reasonably be explained by any exposure map effect. Thus, we conclude that these spurs are real. We return to this issue in

¹ N. Wright Cosmology Calculator via the NASA Extragalactic Database.

² <http://cxc.harvard.edu/ciao/threads/>

³ The radio observation was performed on 1993 May 5, and the reduced radio data were obtained from the NASA Extragalactic Database.

Section 3.4 where we further verify the reality of these spurs through surface brightness profiles derived from unsmoothed data.

We now proceed to discuss the core of this system and, in particular, evidence for radio galaxy–ICM interaction.

3.2 ICM–radio galaxy interaction

In Fig. 2, we show both a raw three-colour X-ray image and an adaptively smoothed total intensity X-ray image of the central regions of the 3C 401 system. As before, the X-ray images have been overlaid with contours of 20-cm radio emission from MERLIN. As is apparent in the raw image, there is a luminous point-like X-ray source at the location of the 3C 401 radio core (see Section 3.3 for more discussion of this source). Although the photon statistics are not good, the ICM emission is clearly not spherically symmetric. In particular, there is a notable deficit of counts 3–5 arcsec north of the central source compared with the same distance east or west of the central source. This deficit is clearly shown in the smoothed total intensity map, which also reveals a similar deficit in the region 3–5 arcsec south of the central source. In other words, there is a strong nuclear bar apparent, with a position angle orthogonal to the radio axis.

Furthermore, careful inspection of the raw image reveals hints of a cone-like structure bounding the northern radio lobe. However, this structure does not appear to survive the adaptive smoothing process, and so its reality cannot be confirmed.

We further investigate these features by forming radial surface brightness profiles. Fig. 3(a) shows the surface brightness profile within quadrants that are centred on the radio axis of 3C 401 (the on-axis profile; dashed line), as well as the profile within the orthogonal quadrants (the off-axis profile; solid line). The nuclear bar-like structure gives rise to a factor of 2 enhancement in the off-axis surface brightness at the smallest radii probed in our surface brightness analysis (seven pixels or 3.5 arcsec). There are other subtle differences between the two radial profiles in the form of relative enhancements in the off-axis profile at 15 and 22 arcsec. These differences, while statistically significant with respect to Poisson

noise, have no obvious corresponding features in either the raw or the smoothed X-ray image. Deeper X-ray images will be required to assess the nature of these particular deviations from circular symmetry.

3.3 The nuclear region

A point source is clearly detected coincident with the radio core of 3C 401. Although the spatial resolution of *Chandra*/ACIS is approximately 2 kpc at the distance of 3C 401, it seems likely that we are detecting the X-ray emission from the active galactic nucleus itself. Using a smaller-than-usual extraction region (1 arcsec radius) in order to separate this source from the surrounding ICM emission, we detect 385 photons in this source, approximately 10–20 per cent of which are accounted for by a reasonable extrapolation of the underlying ICM surface brightness profile. We have searched for but fail to detect temporal variability of this central source. However, our limits on temporal variability are weak because of the limited photon statistics – inspection of the light curve suggests that the source has not varied by more than 30 per cent on the time-scale of the total observation length (1.2×10^5 s), and has not varied by more than a factor of 2 on a time-scale of 10^4 s.

Using our small extraction radius, we have extracted a time-averaged spectrum of this central source. We produce a ‘background’ spectrum from a region offset by 3 arcsec in the western direction. Therefore, in an attempt to isolate the pure nuclear spectrum, the background spectrum also includes thermal emission from the ICM immediately neighbouring the nuclear source. The source spectrum was then binned so as to contain at least 15 photons per energy bin, hence allowing the use of χ^2 statistics.

The 0.5–6 keV nuclear spectrum can be adequately fitted with either a power law or thermal plasma model modified by the effect of Galactic absorption ($N_{\text{H}} = 6.8 \times 10^{20} \text{ cm}^{-2}$) and absorption by contaminants on the ACIS filter (modelled with the ACISABS model). Note that there are inadequate numbers of photons above 6 keV to allow meaningful extension of these fits to higher energies. Best-fitting parameters for the power-law fits are: photon index

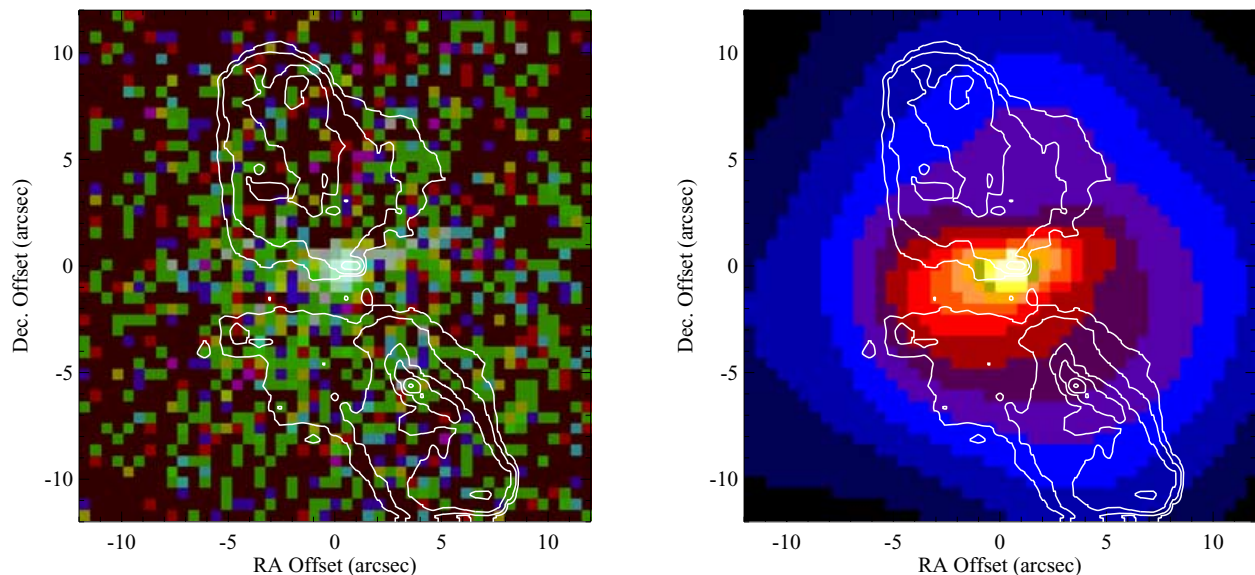


Figure 2. Left panel: Three-colour raw photon image of the central 24×24 arcsec² regions of the 3C 401 system overlaid with contours of 20-cm radio emission from MERLIN. The nucleus of 3C 401 lies at the centre of this image and is coincident with the bright point X-ray source. Right panel: Adaptively smoothed total intensity image of this region. The anticoincidence between the radio lobes and the X-ray emission is evident and results in the formation of a central X-ray bar. Please note that the colour image is only available in the electronic publication.

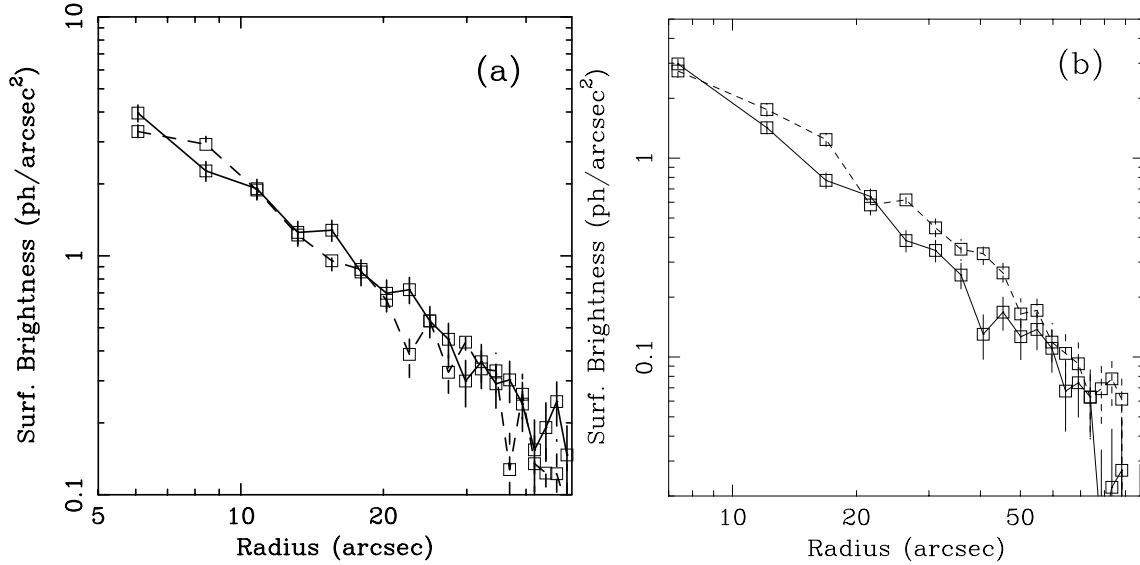


Figure 3. (a) X-ray surface brightness profiles for a back-to-back pair of quadrants that include the radio lobes (dashed line) and the orthogonal pair of quadrants that avoid the radio lobes (solid line). (b) X-ray surface brightness profile analysis using eight 45 degree sectors centred on 3C 401. The solid line shows the profile averaged over the four alternating sectors that avoid the spurs of the cross-like structure seen in Fig. 1. The dashed line shows the profile for the complementary sectors that are coincident with the spurs. The clear excess seen in this latter profile verifies that the cross-like structure is not an artefact of the adaptive smoothing procedure.

$\Gamma = 1.89^{+0.27}_{-0.21}$, intrinsic (redshifted) absorption $N_{\text{H}_z} < 1.0 \times 10^{21} \text{ cm}^{-2}$, observed 0.5–10 keV flux $F_{0.5-10} = 5.5 \times 10^{-14} \text{ erg cm}^{-2} \text{ s}^{-1}$, and intrinsic (unabsorbed) 0.5–10 keV luminosity $L_{0.5-10} = 7.1 \times 10^{42} \text{ erg s}^{-1}$, with a goodness-of-fit parameter $\chi^2/\text{d.o.f.} = 18.4/19$.

The power-law model will be appropriate if we are, indeed, observing AGN emission. However, the possibility remains that this central source could be the compact (unresolved) core of thermal emission from the hot gas halo. Indeed, fitting such a model to the data using the MEKAL model encoded in the XSPEC spectral fitting package (version 11.3.0; Mewe, Gronenschild & van den Oord 1985; Mewe, Lemen & van den Oord 1986; Kaastra 1992; Liedahl, Osterheld & Goldstein 1995) results in a fit that is almost as good as (and statistically indistinguishable from) the power-law model. Best-fitting parameters for this thermal plasma model are: plasma temperature $kT = 4.9^{+2.5}_{-1.8} \text{ keV}$, plasma abundance $Z < 2.6 Z_{\odot}$, intrinsic (redshifted absorption) $N_{\text{H}_z} < 5 \times 10^{20} \text{ cm}^{-2}$, observed 0.5–10 keV flux $F_{0.5-10} = 5.1 \times 10^{-14} \text{ erg cm}^{-2} \text{ s}^{-1}$, and intrinsic (unabsorbed) 0.5–10 keV luminosity $L_{0.5-10} = 6.7 \times 10^{42} \text{ erg s}^{-1}$, with a goodness-of-fit parameter $\chi^2/\text{d.o.f.} = 21.3/18$. The emission measure suggested by this spectral fit is $\text{EM} = 4.1 \times 10^{65} \text{ cm}^{-3}$. If we make the simple and conservative approximation that this thermal plasma uniformly fills a sphere of the size of our extraction region, this emission measure implies a plasma density of $n > 0.25 \text{ cm}^{-3}$, and a bremsstrahlung cooling time-scale of $t_{\text{brems}} < (1-2) \times 10^8 \text{ yr}$. Thus, if this central source is indeed a dense gaseous core, it possesses a cooling time-scale that is much shorter than any realistic age of this cluster.

3.4 The surrounding cluster

Finally, we discuss the gross properties of the ICM emission. We extracted a spectrum from a region centred on 3C 401 with an extraction radius of 32 arcsec (108 kpc). A background spectrum was formed from blank sky observations. After background subtraction, this spectrum possesses 3360 photons. After binning the spectrum

to at least 15 photons per energy bin, we fit the 0.5–8 keV spectral data with a thermal plasma model modified for the effects of Galactic and instrumental absorption (as discussed in Section 3.3). The best-fitting parameters are: plasma temperature $kT = 2.9 \pm 0.3 \text{ keV}$, plasma abundance $Z = 0.43^{+0.20}_{-0.16} Z_{\odot}$, observed 0.5–10 keV flux $F_{0.5-10} = 3.7 \times 10^{-13} \text{ erg cm}^{-2} \text{ s}^{-1}$, and intrinsic (unabsorbed) 0.5–10 keV luminosity $L_{0.5-10} = 5.6 \times 10^{43} \text{ erg s}^{-1}$, with a goodness-of-fit parameter $\chi^2/\text{d.o.f.} = 116/120$. The emission measure for this plasma is measured to be $\text{EM} = 4.3 \times 10^{66} \text{ cm}^{-3}$.

It is also interesting to examine the spatial structure of the cluster. By combining the two radial surface brightness profiles discussed in Section 3.2 (also Fig. 3), we have produced the azimuthally averaged surface brightness profile. To this profile, we fit a standard β model in which the surface brightness is given by

$$S(r) = \frac{S_0}{[1 + (r/r_0)]^{3\beta-1/2}}. \quad (1)$$

In a free fit, we obtain $r_0 = 36 \pm 8 \text{ kpc}$ and $\beta = 0.46^{+0.03}_{-0.02}$ ($\chi^2 = 11.4$ for 17 d.o.f.). This is a rather flat density profile and small core radius for such a cluster to possess. If we fix $\beta = 0.67$, the canonical value measured in rich clusters of galaxies, the fit is substantially worse ($\chi^2 = 80$ for 18 degrees of freedom) as a result of an underprediction of surface brightness at the smallest radii ($< 5 \text{ arcsec}$) and largest radii ($> 30 \text{ arcsec}$) and an overprediction of the surface brightness in the range 10–20 arcsec.

Inverting equation (1) to give the radial dependence of the volume emissivity, and normalizing using the value of EM determined from the spectral fit allows us to deduce the approximate radial run of density $n(r)$ and pressure $p(r)$ (assuming that the ICM is isothermal with $kT = 2.9 \text{ keV}$). The result of this exercise is

$$n(r) = 1.8 \times 10^{-2} \left[1 + \left(\frac{r}{36 \text{ kpc}} \right)^2 \right]^{-3\beta/2} \text{ cm}^{-3} \quad (2)$$

and

$$p(r) = 8.3 \times 10^{-11} \left[1 + \left(\frac{r}{36 \text{ kpc}} \right)^2 \right]^{-3\beta/2} \text{ erg cm}^{-3}. \quad (3)$$

Knowing the absolute values of density and pressure is essential for examining the energetics of the radio galaxy interaction, a topic that we shall address in the next section.

We finish our discussion of surface brightness profiles by returning to the issue of the large-scale spurs or cross-like structure noted in the adaptively smoothed surface brightness map (Fig. 1). Owing to the four-fold symmetry, we do not expect these features to be clearly revealed in the quadrant analysis presented above. To examine a putative structure with four-fold symmetry requires that we perform the following tailored surface brightness profile analysis. We divide the image plane into eight equal and non-overlapping 45 degree sectors centred on the core of 3C 401. This ‘wheel’ of sectors is aligned so that the radio axis of 3C 401 lies on the mid-line of one back-to-back pair of sectors. We then form an average radial surface brightness profile using the four (alternating) sectors that lie either along or perpendicular to the radio axis (Fig. 3b; dashed line). The adaptively smoothed image suggests that these sectors should coincide with the four spurs of the cross-like structure. We compare this with the average radial surface brightness profile using the other four sectors, which, according to the adaptively smoothed image, should lie in the inter-spur gaps (Fig. 3b; solid line). This analysis reveals a clear excess of counts in the on-spur surface brightness profile as compared with the off-spur case at radii of 20–50 arcsec (70–170 kpc). Thus, we conclude that the cross-like structure is not an artefact of the adaptive smoothing.

4 DISCUSSION

Our *Chandra* observations have revealed three striking aspects of the 3C 401 system. First, there is clear evidence for an ongoing interaction between 3C 401 and the ICM of its surrounding galaxy cluster. The most obvious manifestation of this interaction is the nuclear bar (with radius of ~ 10 arcsec/35 kpc) that lies orthogonal to the axis of the MERLIN radio lobes. Guided by observations of radio galaxy–ICM interactions in the Local Universe ($z < 0.1$), it seems very likely that this structure results from the formation of ICM cavities by the expanding radio lobes. The detailed anticoincidence between the X-ray surface brightness and the radio surface brightness seen in 3C 401 supports this hypothesis. Using our estimates of the ICM pressure, we can make a crude estimate for the mechanical power required to inflate these radio lobes. The total energy required to inflate the two lobes is $E \sim 1.5 \times 10^{59}$ erg, where we have approximated each lobe as a sphere with radius 5 arcsec and have taken the required energy to be $E \sim 2pV$, where V is the volume of the lobe. The lifetime of the source is likely to be of the order of the ICM sound crossing time of one radio lobe, $t \sim 1.7 \times 10^{15}$ s. Thus, the time-averaged power required to inflate these radio lobes against the pressure of the ICM is $P = E/t \sim 1 \times 10^{44}$ erg s $^{-1}$. This is very close to the measured X-ray luminosity of the ICM, showing that the radio galaxy can have a major impact on the energetics of the ICM in this source if the mechanical energy can be thermalized efficiently. Taking the spatially integrated 1.4-GHz flux to be 4.7×10^{-23} erg s $^{-1}$ (Kellerman et al. 1969), we estimate the radio power to be $\nu L_\nu \approx 7 \times 10^{42}$ erg s $^{-1}$. This places the 3C 401 cluster near the correlation between the mechanical energy inferred to be inside these cavities and the current radio power level (Bîrzan et al. 2004). Consistency with this correlation means

that the current radio source contains sufficient mechanical energy to create these cavities (assuming the theoretical expectation of a 1–10 per cent efficiency for converting the total radio source mechanical energy into radio-frequency luminosity; Bicknell, Dopita & O’Dea 1997).

Secondly, we have noted a larger-scale cross-like structure extending to distances of ~ 50 arcsec (170 kpc) from the centre of the cluster and also aligned with the radio axis of 3C 401. While the reality of this feature appears to be robust, its interpretation is not clear. The coincidence between the orientation of this structure and the radio axis of 3C 401 suggests that this might also be due to radio plasma interaction with the ICM, although the possibility remains that the cross-like structure is caused by unrelated dynamical processes (e.g. subcluster mergers). If it is indeed due to interaction with 3C 401, two possibilities arise. If this ICM structure is caused by two pairs of ‘ghost cavities’, then they are amongst the largest known. Using the same assumptions as in the paragraph above to assess the energetics of these ghost cavities, we estimate that 3C 401 had to have a period about 300 Myr ago in which its mechanical power was $(2\text{--}5) \times 10^{44}$ erg s $^{-1}$ (i.e. a factor of a few greater than the present). While this explanation for the ICM cross has the appeal that ghost cavities are structures that are *known* to exist in some clusters, it does not naturally explain the four-fold symmetry of this structure (the two pairs of ghost cavities would have to lie at roughly the same distance from 3C 401 and have axes that are perpendicular).

This leads us to speculate that the ICM cross is actually due to a high-amplitude global oscillation mode (most likely a low- l internal gravity mode) excited by a previous outburst from 3C 401. The theory of such oscillations has been developed by Balbus & Soker (1990) and Lufkin, Balbus & Hawley (1995), although these authors envisage the excitation of internal g modes through a resonant interaction with orbiting galaxies, not through an explosive central event. A detailed theoretical investigation of this possibility, including predicted maps of ICM surface brightness and temperature for different modes, is beyond the scope of this paper. At this stage, we note that the oscillation period of such a mode will be a factor of a few longer than the sound crossing time of the region, and the energy of the mode will be of the same order as that estimated above for the ghost cavity scenario. However, it is likely that only a modest fraction of the total energy from the radio galaxy outburst would end up in such a mode, with p modes likely carrying away the majority of the energy of the initial blast. Hence, within this scenario, 3C 401 would likely have exceeded a mechanical luminosity of 10^{45} erg s $^{-1}$ during its past phase of activity. Deeper imaging of this field (most likely with *XMM-Newton*) will be required to study the ICM cross structure in more detail and to distinguish between (or disprove) the ghost cavity and global mode scenarios.

The final striking aspect of this system is the unusual surface brightness distribution of the cluster – we measure a core radius of $r_0 = 36$ kpc and $\beta = 0.46$, substantially flatter than the typical $\beta = 0.67$ found in many clusters of a comparable or greater mass. However, this is quite similar to the value of β found in low-mass clusters and groups (Osmond & Ponman 2004, and references therein), a result that is taken as evidence for the enhanced importance of excess entropy in these low-mass systems. Whether the 3C 401 cluster really is anomalous in having a flat profile for its mass requires further study with deeper X-ray imaging. In particular, one may be concerned that we are not obtaining a true measure of the value of β given that the central region of the cluster is morphologically complex and that we cannot constrain the ICM surface brightness profile

beyond about 170 kpc. If the flat profile is confirmed, it is tempting to interpret this as a sign of particularly strong ICM heating and entropy injection, as might be expected for a cluster whose ICM is still in the process of forming. Indeed, we proposed to observe this radio galaxy/ICM system with *Chandra* because previous work (Harvanek et al. 2001; Harvanek & Stocke 2002) presented significant evidence linking intermediate FRI/FRII radio galaxies to the formation of a dense ICM in the cluster that surrounds them.

5 CONCLUSIONS

Chandra imaging spectroscopy of the intermediate FRI/FRII radio galaxy 3C 401 reveals clear signs of an interaction between the radio galaxy and the ICM of its surrounding cluster. Although we do not see well-defined ICM cavities (most likely as a result of the limited number of photons in our image), the flattening of the central X-ray isophotes strongly suggests that the radio lobes are indeed evacuating cavities within the ICM with a radius of 15–20 kpc. There are also deviations from spherical symmetry on much larger spatial scales (100 kpc or more) that reveal themselves as a cross-like structure in the low surface brightness regions of the ICM. It is tantalizing to speculate that a previous, much more powerful, period of activity from 3C 401 created these large-scale disturbances. While this large-scale cross-like pattern might be caused by a pair of ghost cavities related to previous activity, the symmetry of this structure leads us to speculate that the ICM atmosphere is executing large-amplitude, low- l g-mode oscillations. Deeper imaging of this field (with either a very long *Chandra* observation or a moderately deep *XMM-Newton* observation) is required to probe these possibilities further.

The ICM possesses a temperature of $kT \approx 2.9$ keV and a 0.5–10 keV luminosity of $L_{0.5-10} = 5.6 \times 10^{43}$ erg s $^{-1}$, placing it firmly on the standard L – T relationship of Horner (2002). This cluster also possesses an X-ray luminosity typical for its cluster richness (B_{gg} value; Yee & Ellington 2003), although its T_X is nearly a factor of 2 below that expected for its richness (Yee & Ellington 2003). In addition, its surface brightness profile is unusually flat. When parametrized by a standard King-type model, the ICM possesses $\beta = 0.46$, much flatter than the normal $\beta = 0.67$ found in clusters of comparable or greater mass. These unusual ICM features may all be due to the unusually large radio power level of the central galaxy for a cluster with a dense ICM. However, because this analysis uses a total of only a few thousand X-ray photons, we worry that the ICM surface brightness distribution may not have been measured robustly as yet.

This system is ripe for deeper X-ray imaging spectroscopy, either with a long *Chandra* stare or a moderately long *XMM-Newton* observation. With such data, we will be able to search for the well-defined ICM cavities that probably encase the currently active radio lobes, study the cross-like structure on 170 kpc scales, and

constrain the ICM surface brightness profile significantly beyond 100 kpc. New data of this type will take studies of the current radio galaxy–ICM interaction as well as the ICM thermodynamics of the 3C 401 system to the next level.

ACKNOWLEDGMENTS

We thank Steve Balbus, Mitch Begelman and Andy Fabian for stimulating discussions through the course of this work. We acknowledge support from *Chandra* Cycle-3 Guest Observer Program under grant G02-3143X and the National Science Foundation under grant AST0205990.

REFERENCES

- Balbus S. A., Soker N., 1990, *ApJ*, 357, 353
 Benson A. J., Bower R. G., Frenk C. S., Lacey C. G., Baugh C. M., Cole S., 2003, *ApJ*, 599, 38
 Bicknell G. V., Dopita M. A., O’Dea C. P., 1997, *ApJ*, 485, 112
 Binney J., 2004, *Phil. Trans. R. Soc.*, in press (astro-ph/0407238)
 Birzan L., Rafferty D. A., McNamara B. R., Wise M. W., Nulsen P. E. J., 2004, *ApJ*, 607, 800
 Blanton E. L., Sarazin C. L., McNamara B. R., Wise M. W., 2001, *ApJ*, 558, L15
 Choi Y. Y., Reynolds C. S., Heinz S., Rosenberg J. L., Perlman E. S., Yang J., 2004, *ApJ*, 606, 185
 David L. P. et al., 2001, *ApJ*, 557, 546
 Fabian A. C., 1994, *ARA&A*, 32, 277
 Fabian A. C. et al., 2000, *MNRAS*, 318, L65
 Fabian A. C. et al., 2002, *MNRAS*, 331, L35
 Fabian A. C. et al., 2003, *MNRAS*, 344, L43
 Harvanek M., Stocke J. T., 2002, *AJ*, 124, 1239
 Harvanek M., Ellington E., Stocke J. T., Rhee G., 2001, *AJ*, 122, 2874
 Heinz S., Choi Y. Y., Reynolds C. S., Begelman M. C., 2002, *ApJ*, 569, L79
 Horner D., 2002, PhD thesis, Univ. Maryland
 Jones C. et al., 2002, *ApJ*, 567, L115
 Kaastra J. S., 1992, An X-ray Spectral Code for Optically-Thin Plasmas. Internal SRON–Leiden Report, updated version 2.0
 Kellerman K. I., Pauliny-Toth I. I. K., Williams P. J. S., 1969, *ApJ*, 157, 1
 Liedahl D. A., Osterheld A. L., Goldstein W. H., 1995, *ApJ*, 438, L115
 Lufkin E. A., Balbus S. A., Hawley J. F., 1995, *ApJ*, 446, 529
 McNamara B. R. et al., 2000, *ApJ*, 534, L135
 McNamara B. R. et al., 2001, *ApJ*, 562, L149
 Mewe R., Lemen J. R., van den Oord G. H. J., 1986, *A&AS*, 65, 511
 Nulsen P. E. J. et al., 2002, *ApJ*, 568, 163
 Osmond J. P. F., Ponman T. J., 2004, *MNRAS*, 350, 1511
 Smith D. A., Wilson A. S., Arnaud K. A., Terashima Y., Young A. J., 2002, *ApJ*, 565, 195
 Spergel D. N. et al., 2003, *ApJS*, 148, 175
 Yee H. K. C., Ellington E., 2003, *ApJ*, 585, 215

This paper has been typeset from a $\text{\TeX}/\text{\LaTeX}$ file prepared by the author.